axisymmetric contoured nozzles are unacceptable, moderate angle (10°) conical expansions provide a reasonable compromise between freezing efficiency, boundary-layer losses, and shock losses. Experiments have shown that mixing of the complex exit flow from a screen nozzle comprised of such elements effectively takes place in a downstream distance of 100 element spacings. At this point regular and random density disturbances have decayed to less than 1%. This is in general agreement with both wave-like and wake-like models for the process and is a level that allows high beam quality in a large $N_2$-$CO_2$ GDL. The optical gain at this location is accurately predicted by calculations based on the assumption of instantaneous mixing at the nozzle exit.

The calculations show that the performance of the screen nozzle is improved by operating it at a higher $p_o d^*$ than the optimum value for its 2-D counterpart. The over-all pressure recovery of a screen nozzle system may then actually exceed that for the 2-D grid nozzle, while relative gain and laser energy available penalties at least as low as 30% and 10% respectively, can be expected. Performance may be further improved for a specific application through a systematic optimization of screen nozzle geometry, area ratio, gas mixture, optical axis, and operating conditions. Screen nozzles thus offer extreme simplicity and flexibility at little performance cost.

## References

[1] Russell, D. A., "Fluid Mechanics of High Power Grid Nozzle Lasers," AIAA Paper 74-223, Washington, D.C., 1974.

[2] Greenberg, R. A., et al., "Rapid Expansion Nozzles for Gas Dynamic Lasers," *AIAA Journal*, Vol. 10, Nov. 1972, pp. 1494–1498.

[3] Director, M. N., "Aerodynamic Parameters Affecting Practical Gas Dynamic Laser Design," AIAA Paper 73-626, Palm Springs, Calif., 1973.

[4] Simons, G. A., "Decay of a Diamond Shock Pattern," *AIAA Journal*, Vol. 10, Aug. 1972, pp. 1037–1043.

[5] Reshotko, E. and Haefeli, R. C., "Investigation of Axially Symmetric and Two-Dimensional Multinozzles for Producing Supersonic Streams," RM E52H28, Oct. 1952, NACA.

[6] Foelsch, K., "The Analytical Design of an Axially-Symmetric Laval Nozzle for a Parallel and Uniform Jet," *Journal of the Aeronautical Sciences*, March, 1949, pp. 161–188.

[7] Cohen, C. B. and Reshotko, E., "The Compressible Laminar Boundary Layer with Heat Transfer and Arbitrary Pressure Gradient," Rept. 1294, 1956, NACA.

[8] Swain, L. M., "On the Turbulent Wake Behind a Body of Revolution," *Proceedings of the Royal Society of London*, Series A, Vol. 125, 1929, pp. 647–659.

[9] Schlichting, H., *Boundary-Layer Theory*, 6th ed., McGraw-Hill, New York, 1968.

[10] Monsler, M. J. and Greenberg, R. A., "The Effects of Boundary Layers on the Gain of a Gas-Dynamic Laser," AIAA Paper 71-24, New York, N.Y., 1971.

[11] Townsend, A. A., *The Structure of Turbulent Shear Flow*, Cambridge University Press, New York, 1956.

[12] Newton, J., Pindroh, A., and Byron, S., "$CO_2$ Optical Gain in Gasdynamic Lasers Using $CO_2/N_2/H_2O/CO/H_2$ Mixtures," Mathematical Sciences NW, Inc., USAF Rept. AFWL-TR-71-105, July 1971.

[13] Chernov, L. A., *Wave Propagation in a Random Medium*, McGraw-Hill, New York, 1960.

[14] Russell, D. A., Buonadonna, V. R., and Jones, T. G., "Double Expansion Nozzles for Shock Tunnels and Ludwieg Tubes," in *Recent Developments in Shock Tube Research*, edited by Bershader and Griffith, Stanford University Press, 1973.

MAY 1975 AIAA JOURNAL VOL. 13, NO. 5

# Shape Change and Conduction for Nosetips at Angle of Attack

JIN H. CHIN*
*Lockheed Missiles & Space Co., Inc., Sunnyvale, Calif.*

**A computerized procedure is developed to determine the three-dimensional thermal response of ablating bodies. The formulation is based upon a spherical, transformed, moving coordinate grid system. An expression for the generalized heat flux for anisotropic media is derived. A lumped capacitance concept is invoked to derive the nodal point heat balance equation. The instantaneous body shape governs the environment predictions. The effects of streamline spreading are taken into account along the windward and leeward rays. The pressure and heat transfer distributions for other azimuthal planes are computed according to a principle of similarity with respect to the local orientation angle. Validating and illustrative results are given. Application of the procedure to graphite nosetip analysis demonstrates that a significant asymmetry is developed in shape and internal temperatures for nosetips at angle of attack.**

## Nomenclature

$a, b, c$ = principal directions
$a_{pq}$ = $\mathbf{p}\cdot\mathbf{q}$, e.g., $a_{c\xi} = \mathbf{c}\cdot\boldsymbol{\xi}$
$A$ = heat transfer area
$c$ = specific heat
$C_H$ = zero blowing heat transfer coefficient
$C_\theta$ = $(\partial r/\partial\theta)_\phi$
$C_\phi$ = $(\partial r/r\sin\theta\,\partial\phi)_\theta$
$Fo$ = Fourier number
$g$ = $h_\beta/r_c$; generalized conductivity, Eq. (7)
$G$ = generalized conductance
$h$ = scale factor for curvilinear coordinate: $h_\xi = \Delta/(1+C_\theta{}^2+C_\phi{}^2)^{1/2}$, $h_\theta = r$, $h_\phi = r\sin\theta$
$h_\beta$ = spreading coordinate
$k$ = thermal conductivity
$K_1, K_2$ = principal curvatures
$\dot{m}_t$ = total mass ablation rate
$M$ = Mach number
$p$ = pressure; index for $c, a, b$
$q$ = heat flux; index for $\xi, \theta, \phi$
$r$ = spherical radial coordinate
$r_c$ = cylindrical radial coordinate
$r_i$ = $r$ for inner boundary
$r_s$ = $r$ for nosetip surface
$Re$ = Reynolds number

Presented as Paper 74-516 at the AIAA 7th Fluid and Plasma Dynamics Conference, Palo Alto, California, June 17–19, 1974; submitted June 7, 1974; revision received November 11, 1974. This work was supported by the LMSC Independent Development Program and by Navy Contract N00030-72C-0108.

Index categories: Material Ablation; Heat Conduction; Entry Vehicles and Landers.

* Staff Engineer, Aero-Thermodynamics Department, Engineering Technology. Member AIAA.

$R_N$ = initial nose radius
$R_\phi$ = $R_2 \cos\theta_e$
$R_1, R_2$ = principal radii of curvature
$s$ = wetted distance from stagnation point
$s_\epsilon$ = small value of $s$, $s_\epsilon/R_2 \ll 1$
$t$ = time
$T$ = temperature
$T_i$ = initial temperature
$u$ = velocity
$V$ = volume; general variable
$x, y, z$ = Cartesian coordinates
$\alpha$ = angle of attack
$\Delta$ = shell region thickness
$\theta$ = angle between position vector and $z$-axis; momentum thickness
$\theta_c$ = cone half-angle
$\theta_e$ = body angle with respect to wind axis
$\theta_u$ = local orientation angle
$\xi$ = transformed coordinate, Eq. (1)
$\rho$ = density
$\phi$ = spherical azimuthal angle
$\phi_c$ = cylindrical azimuthal angle

*Subscripts*

$a, b, c$ = principal directions
$m$ = node $m$
$n$ = time step $n$
$o$ = stagnation point
$\gamma$ = direction $\gamma$
$\infty$ = freestream

## I. Introduction

TO assess the thermal and structural integrity of the nosetip of re-entry vehicles, it is important to determine the shape change history and the development of the internal temperature of the nosetip along its trajectory. Previous works related to nosetip thermal response are primarily for axisymmetric (2-D) nosetips at zero incidence.[1-4] These works consider either shape change alone[1] or coupled to internal conduction analysis, which requires a long computer run time and large computer storage.[2-4] More recently, the effects of angle of attack on nosetip shape change have been studied.[5-7] Discussions also are given on the various factors affecting shape change predictions[6] and on the design problems peculiar to graphite nosetips in their relationship to over-all re-entry vehicle thermal/structural capability.[8]

In the 2-D, or axisymmetric, program (GRANT) of Ref. 4, the internal temperature field is computed by finite difference with a time-invariant rectangular grid system. As the surface ablates, the number of nodal points changes as the surface moves across the grid intersections. The bookkeeping procedure for boundary movement calculations is very complicated. The purpose of the present paper is to present the formulation of a new 3-D thermal response program (GRANT3D), based upon an alternate grid system in terms of the spherical, transformed, moving coordinates. With this method, the boundary motion calculation is simplified considerably. The total number of nodal points required for a given problem may be significantly decreased, thus reducing the computer run time and storage. Examples of computed results and comparison with data are given.

## II. Analysis

### A. Spherical, Transformed, Moving Coordinates

Figure 1 shows a schematic of a shell nosetip and defines the spherical coordinates. The spatial coordinates $(r, \theta, \phi)$ are transformed into $[\xi, \theta, \phi; \Delta(\theta, \phi, t)]$ according to the following expression:

$$\xi = [r - r_i(\theta, \phi)]/\Delta(\theta, \phi, t) \tag{1}$$

In terms of this moving coordinate system, the inner boundary and the surface always correspond to $\xi = 0$ and $\xi = 1$, respectively. The region of interest $[0 \leq \xi \leq 1, 0 \leq \theta \leq \theta_{max}, 0 \leq \phi \leq \phi_{max}; \Delta(\theta, \phi, t)]$ is then subdivided by uniform or nonuniform

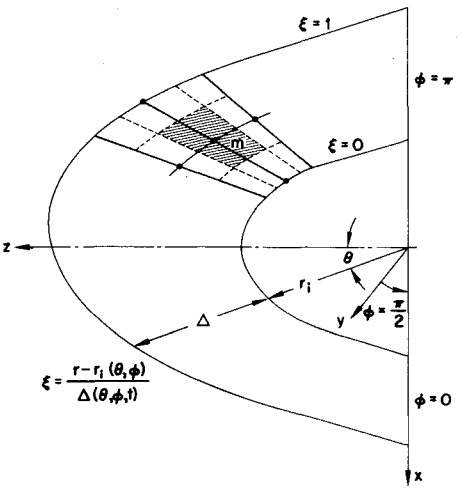


**Fig. 1 Spherical, transformed, moving coordinates.**

increments in $\xi$, $\theta$ and uniform increments in $\phi$. For problems with complete asymmetry and with a plane of symmetry, $\phi_{max}$ equals $2\pi$ and $\pi$, respectively. As the nosetip ablates, the volume associating with a node decreases proportionally.

### B. Conduction Calculations

Single-material nosetips are considered in the present study. Anisotropic and temperature-dependent properties are permitted.

*Generalized heat fluxes*

For general anisotropic materials, the orientation of the conductivity principal axes may be arbitrary. The unit vectors **c**, **a**, **b** associating with the principal axes are mutually perpendicular. For graphite nosetips, however, **c** is generally aligned with the nosetip axis and $k_a \approx k_b$. It is then convenient to assume **c**, **a**, and **b** to be aligned with the $z$-, $x$-, and $y$-axis, respectively. The Cartesian components for the unit vectors of interest are summarized by Eq. (2),

$$\begin{bmatrix} \mathbf{r} \\ \boldsymbol{\theta} \\ \boldsymbol{\phi} \\ \mathbf{c} \\ \mathbf{a} \\ \mathbf{b} \\ \boldsymbol{\xi} \end{bmatrix} = \begin{bmatrix} \sin\theta\cos\phi & \sin\theta\sin\phi & \cos\theta \\ \cos\theta\cos\phi & \cos\theta\sin\phi & -\sin\theta \\ -\sin\phi & \cos\phi & 0 \\ 0 & 0 & 1 \\ 1 & 0 & 0 \\ 0 & 1 & 0 \\ \xi_x & \xi_y & \xi_z \end{bmatrix} \tag{2}$$

where $\boldsymbol{\xi}$ is a unit normal to the $\xi$-level surface and

$$\xi_x = \frac{(\sin\theta - C_\theta\cos\theta)\cos\phi + C_\phi\sin\phi}{(1 + C_\theta^2 + C_\phi^2)^{1/2}}$$

$$\xi_y = \frac{(\sin\theta - C_\theta\cos\theta)\sin\phi - C_\phi\cos\phi}{(1 + C_\theta^2 + C_\phi^2)^{1/2}}$$

$$\xi_z = \frac{\cos\theta + C_\theta\sin\theta}{(1 + C_\theta^2 + C_\phi^2)^{1/2}}$$

The trio unit vectors $\boldsymbol{\xi}$, $\boldsymbol{\theta}$, $\boldsymbol{\phi}$ generally do not form an orthogonal set. However, the nonzero determinant of their Cartesian components establishes their linear independency. Thus, any vector may be uniquely expressed as a linear function of the trio $\boldsymbol{\xi}$, $\boldsymbol{\theta}$, $\boldsymbol{\phi}$.[9] From elementary calculus, the gradient vector may be expressed as follows:

$$\text{grad } T = \frac{1}{h_\xi} T_\xi \boldsymbol{\xi} + \frac{1}{h_\theta} T_\theta \boldsymbol{\theta} + \frac{1}{h_\phi} T_\phi \boldsymbol{\phi} \tag{3}$$

where $h_\xi$, $h_\theta$, $h_\phi$ are the scale factors for curvilinear coordinates $\xi$, $\theta$, $\phi$, respectively; and $T_\xi$ represents $(\partial T/\partial\xi)_{\theta,\phi}$.

The conductive heat fluxes along the principal directions are given by the following expressions

$$-q_p = k_p T_{x_p}, \quad (p = c, a, b) \tag{4}$$

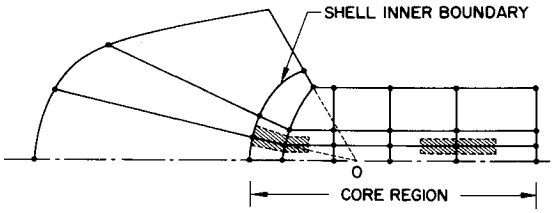


**Fig. 2 Simulation of plug nosetip.**

The gradients in the principal directions may be transformed by the following matrix equation

$$[T_{x_p}] = [a_{pq}][(1/h_q)T_q], \quad (p = c, a, b; q = \xi, \theta, \phi) \tag{5}$$

where, for example, $a_{c\xi} = \mathbf{c} \cdot \boldsymbol{\xi}$, etc., elements of a $3 \times 3$ matrix.

Since the heat flux along direction $\gamma$ is expressible linearly in terms of the components in the principal directions, the following generalized heat flux expression may be derived from Eqs. (4) and (5).

$$-q_\gamma = \sum_{q=\xi,\theta,\phi} G_{\gamma q} T_q \tag{6}$$

where $G_{\gamma q} = g_{\gamma q}/h_q$, and $g_{\gamma q}$ is a generalized conductivity given by Eq. (7).

$$g_{\gamma q} = \sum_{p=c,a,b} k_p a_{pq} a_{p\gamma}, \quad (q = \xi, \theta, \phi) \tag{7}$$

Equation (7) yields, for the set given by Eq. (2) for example

$$g_{\xi\phi} = -k_a C_\phi/(1 + C_\theta^2 + C_\phi^2)^{1/2} \tag{8}$$

which is a member of a set for computation of the heat fluxes in the $\xi$, $\theta$, and $\phi$ directions.

*Lumped capacitance Approximation*

The elementary volume and heat transfer areas are given by the following expressions

$$\begin{aligned} dV &= r^2 \sin\theta \Delta\, d\xi\, d\theta\, d\phi \\ d\mathbf{A}_\xi &= (1 + C_\theta^2 + C_\phi^2)^{1/2} r^2 \sin\theta\, d\theta\, d\phi\, \boldsymbol{\xi} \\ d\mathbf{A}_\theta &= r \sin\theta \Delta\, d\xi\, d\phi\, \boldsymbol{\theta} \\ d\mathbf{A}_\phi &= r\Delta\, d\xi\, d\theta\, \boldsymbol{\phi} \end{aligned} \tag{9}$$

At a given instant of time and in the absence of volumetric source or sink, the energy balance for a control volume may be written as follows

$$\int_{\text{C.V.}} \rho c \left(\frac{\partial T}{\partial t}\right)_x dV = -\oint_{\text{C.S.}} \mathbf{q} \cdot d\mathbf{A} \tag{10}$$

The subscript **x** signifies the basis of a fixed coordinate system. The time derivative is expressible in terms of the transformed coordinates as follows

$$\left(\frac{\partial T}{\partial t}\right)_{r,\theta,\phi} = \left(\frac{\partial T}{\partial t}\right)_{\xi,\theta,\phi} - \xi \left(\frac{\partial \Delta}{\partial t}\right)_{\theta,\phi} \frac{1}{\Delta} \left(\frac{\partial T}{\partial \xi}\right)_{\theta,\phi,t} \tag{11}$$

Now, Eqs. (6), (9), and (11) are substituted into Eq. (10) and a generalized, lumped-capacitance approximation[10] is invoked for the integration over the volume of node $m$ (Fig. 1). The result may be written in the following abbreviated form

$$\rho_m c_m V_m (dT_m/dt) = C_m + Q_m \tag{12}$$

where $C_m$ is the "convection" term from integration of the last term of Eq. (11), and $Q_m$ is the net heat flux entering node $m$. The finite-difference expressions of $C_m$ and $Q_m$, and the numerical treatment of the boundary conditions are discussed in detail in Ref. 11. With the thermal properties evaluated at the present known temperatures, both $C_m$ and $Q_m$ are linear functions of the temperature at node $m$ and its surrounding nodes. An unconditionally stable, alternating direction explicit (ADE) method[4] is used for the timewise integration of Eq. (12). The boundary movement required for evaluation of $C_m$ is calculated, however, by a simple explicit procedure.

*Extension to plug nosetip*

The plug nosetip is simulated by attaching a fixed-boundary core to the moving-boundary shell (Fig. 2). In the core, the effective heat transfer area between two adjacent nodes is perpendicular to the grid connecting them. The temperature gradient along the connecting grid alone is used to compute the heat flux across their common boundary. This approximation is reasonable for a weakly anisotropic medium. To be consistent with the previous method, the fictitious boundary between the shell and core regions is chosen to be a spherical surface.

### C. Environment Prediction

For environmental calculations, it is assumed that the nosetip is symmetric with respect to a pitch plane ($\phi_{\max} = \pi$). This implies that the "effective" wind vector is always parallel to the pitch plane. Without this assumption, the environment prediction is too complicated for practical design calculations. The pressure and heating distributions along the pitch-plane rays (the windward and leeward rays) are computed by the methods of Ref. 4 (with modifications, improvements, and additional options,[11] including laminar, transitional, turbulent, and roughness heating). For angle-of-attack calculations, however, the local radius from the instantaneous wind axis is replaced by the spreading coordinates (or transverse metric coefficient). The environment for the other azimuthal planes is computed by an interpolation procedure.

*Spreading coordinates*

Several methods[12-14] are available for computation of the spreading coordinates. The method of Ref. 14 is adopted. Furthermore, only the streamlines along the windward and leeward rays are considered. Along the pitch plane of symmetry, the streamline momentum equation reduces to the following[14]:

$$\frac{1}{h_\beta}\frac{Dh_\beta}{Ds} = -\frac{\cos\theta_e}{R_1 R_\phi} - \frac{1}{\rho u^2}\left[\left(\frac{1}{h_\beta}\frac{Dh_\beta}{Ds} - \frac{1}{R_\phi}\frac{Dr_c}{Ds}\right) \times \left(-\frac{Dp}{Ds}\right) + \frac{1}{r_c^2}\frac{\partial^2 p}{\partial \phi_c^2}\right] \tag{13}$$

Let $g \equiv h_\beta/r_c$ and assume a modified Newtonian pressure for the evaluation of $\partial^2 p/\partial \phi_c^2$. After a considerable algebra, Eq. (13) is reduced to the following expression

$$\frac{D^2 g}{Ds^2} + a\frac{Dg}{Ds} + (b\tau + \psi)g = 0 \tag{14}$$

where

$$\begin{aligned} \tau &= 1 - \omega,\ \omega = K_2 r_c/\cos\theta_e \\ a &= [(-Dp/Ds)/\rho u^2] + 2\sin\theta_e/r_c \\ b &= [(-Dp/Ds)/\rho u^2](\sin\theta_e/r_c) - (K_1 \cos\theta_e/r_c) \\ \psi &= [2(p_o - p_\infty)/\rho u^2]\sin\theta_e(\cos\theta_e/r_c)^2\,[r_c(D\tau/Ds) + \tau\omega\sin\theta_e] \end{aligned} \tag{15}$$

For axisymmetric bodies, $\tau = \psi = 0$. Near the stagnation point, the limiting form of Eq. (14) yields the following analytical expression[14,11]:

$$g = (s/s_\varepsilon)^{(K_2 - K_1)/K_1}, \qquad (0 \leqq s \leqq s_\varepsilon) \tag{16}$$

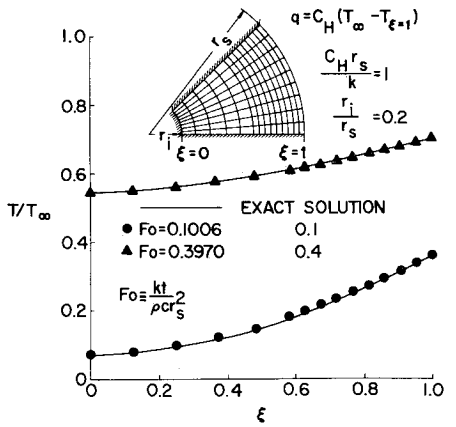


**Fig. 3 Sphere shell, comparison with exact solution.**

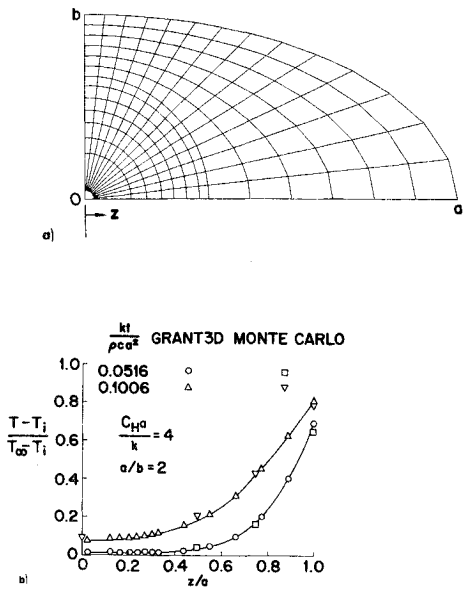


Fig. 4 Prolate spheroid: a) grid system; b) comparison with Monte Carlo results.

The values of $g$ and $Dg/Ds$ at $s_\infty$ obtained from Eq. (16), are used as the initial conditions for the numerical integration of Eq. (14).

*Pressure and heating distributions*

Let $\theta_u$, between the local surface inward unit normal and the wind vector, be termed the local orientation angle. Then the values of $\theta_u$ completely determine the Newtonian or modified Newtonian pressure distribution. For other pressure distribution correlations and for heat transfer, $\theta_u$ is expected to be a dominant correlation variable. The recent results of Refs. 15 and 16 indicate that for sphere cones at various angles of attack the local heat transfer can be correlated with the local pressure (both normalized by the value at the stagnation point), over a one and one-half magnitude in pressure and heat transfer. Thus, a generalized approximation of "similarity with respect to the local orientation angle" may be inferred as follows

$$V(\theta, \phi) = f[\theta_u(\theta, \phi)] \tag{17}$$

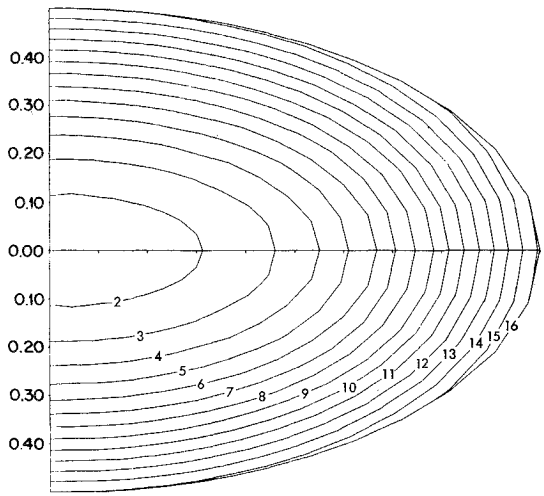

| ISOTHERM | DEG(R) | ISOTHERM | DEG(R) | ISOTHERM | DEG(R) |
|---|---|---|---|---|---|
| 2 | 100 | 7 | 350 | 12 | 600 |
| 3 | 150 | 8 | 400 | 13 | 650 |
| 4 | 200 | 9 | 450 | 14 | 700 |
| 5 | 250 | 10 | 500 | 15 | 750 |
| 6 | 300 | 11 | 550 | 16 | 800 |

Fig. 5 Prolate spheroid isotherm plot.

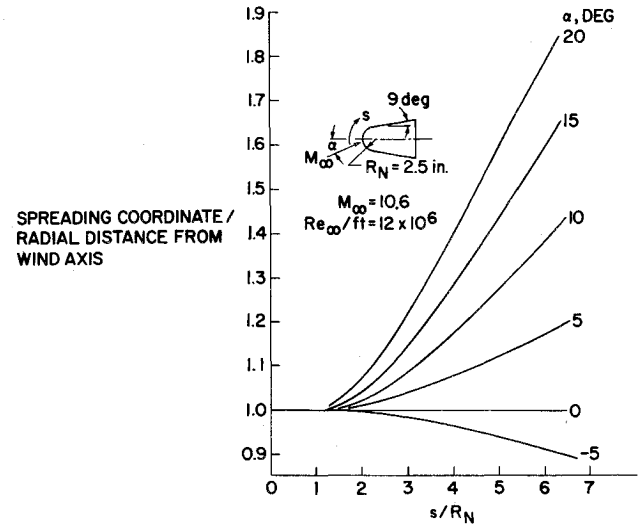


Fig. 6 Variation of spreading coordinates.

where $V(\theta, \phi)$ represents a variable at a point $(\theta, \phi)$ on the nose-tip surface. The function $f$ depends upon $\theta$, freestream variables, and whether the flow is laminar or turbulent. In the region of transitional heating, it is expected that the accuracy of correlation Eq. (17) may decrease; nevertheless, Eq. (17) remains useful in providing a relatively simple estimate of the azimuthal variations.

A very simple form of $f$ corresponds to the following linear relation

$$V(\theta, \phi) = V(\theta, 0) + \frac{V(\theta, \pi) - V(\theta, 0)}{\theta_u(\theta, \pi) - \theta_u(\theta, 0)} [\theta_u(\theta, \phi) - \theta_u(\theta, 0)] \tag{18}$$

The logarithms of pressure and heat transfer coefficient are used in Eq. (18). The quantities $V(\theta, \pi)$ and $V(\theta, 0)$ are evaluated at the pitch plane of symmetry.

### D. Shape Change Calculations

The movement of the surface nodal points is given by the following very simple expression

$$\Delta(\theta, \phi, t_{n+1}) = \Delta(\theta, \phi, t_n) - [(1 + C_\theta{}^2 + C_\phi{}^2)^{1/2} \dot{m}_t(\theta, \phi)/\rho]_{t_n} \Delta t_n \tag{19}$$

where subscript $t_n$ denotes evaluation at time $t_n$. The movement of nodal points is thus along the radial lines (constant $\theta$ and $\phi$).

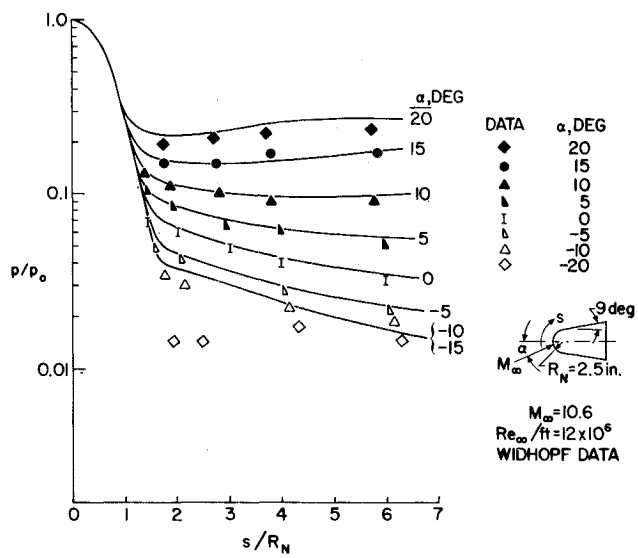


Fig. 7 Pressure distribution, sphere-cone at angle of attack.

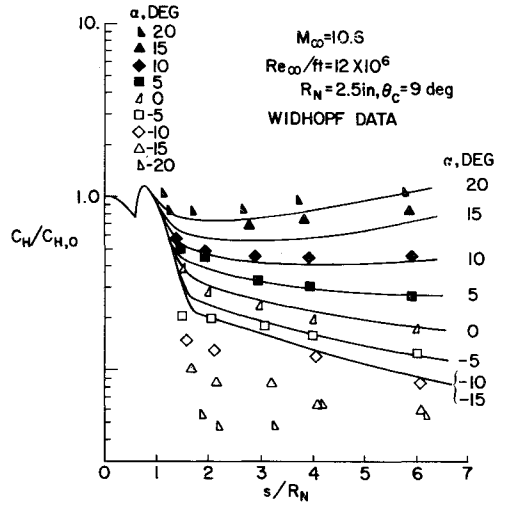


**Fig. 8 Heat transfer distribution, sphere-cone at angle of attack.**

### E. Numerical Description of Surface Contour

From the previous subsections, it is evident that not only $r_i(\theta, \phi)$ and $\Delta(\theta, \phi, t)$ but also their derivatives with respect to $\theta$ and $\phi$ are required to describe the surface contour. A combination of methods[11] is used here. The cubic spline method is found useful for evaluating $C_\phi$; it also gives good $C_\theta$ results for analytical shapes without sharp corners. For ablating bodies with possible sharp corners, the method of straight-line segments provides more consistent results. When the nosetip is sharpened because transition occurs near the stagnation point, a second-order least-squares surface fit of the stagnation region improves the results.

The instantaneous surface contour governs the pressure and heat transfer distributions, which in turn drive the process for shape change and internal conduction. Each step of calculations is subject to uncertainties,[6] the discussion of which is not the objective of the present paper.

## III. Results and Conclusions

To validate the analysis methods, the present computer program (GRANT3D) is used to calculate special problems for which exact or other numerical solutions are available. The first case considered is a sphere shell with an adiabatic inner boundary and the surface exposed to a uniform environment. The computed results (Fig. 3) agree very well with the exact, one-dimensional solution.[17] Another case considered is a prolate spheroid exposed to a uniform environment. The grid geometry is shown in Fig. 4a. A small hole at the center is used to avoid the singular origin of the spherical coordinates. The results compare favorably (Fig. 4b) with those obtained by a Monte Carlo method.[18] Figure 5 is an

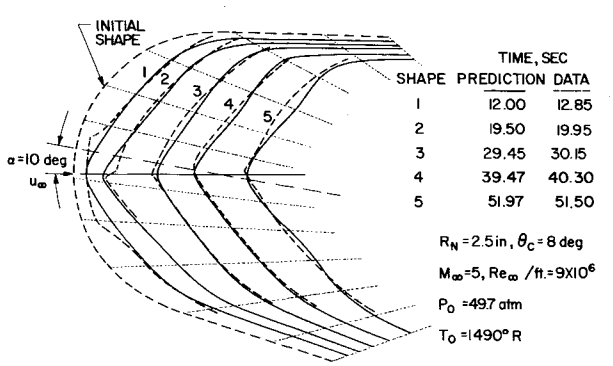


**Fig. 9 Camphor ablation, theoretical, and experimental shapes.**

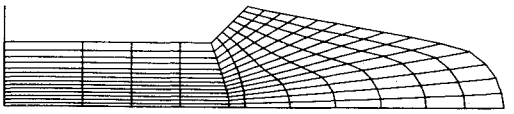

**Fig. 10 Nosetip initial grids.**

isotherm plot indicating a small effect of the hole on the innermost isotherm.

Environment predictions for blunt cones are compared with the data of Ref. 19. Figure 6 shows the ratio of the spreading coordinate to the radial distance from the wind axis. This ratio is considerably larger than unity at large values of $\alpha$ and $s/R_N$. Figures 7 and 8, respectively, compare the pressure and heat transfer coefficient distributions. Reasonable agreement is seen except for the leeward ray at very large angles of attack. Under this situation, however, the boundary layer is separated and the heat transfer is relatively low.

Shape change predictions for camphor ablation are compared with the data of Ref. 20 in Fig. 9. Quasisteady camphor ablation[20] (no conduction calculation) is assumed. Very coarse grids (dotted radial lines, Fig. 9) are employed. The PANT $Re_\theta$ transition correlation[21] is used with an effective transition roughness height of 0.001 in. An effective roughness height of 0.0022 in. is used for turbulent heating increment computations. The comparison is favorable. The neglect of roughness-growth in the calculations explains the difference in shape at early times.

Example computation results of graphite nosetip at angle of of attack are given in Figs. 10–15. Five azimuthal planes are used to evaluate the 3-D effects. Figure 10 shows the initial grid system of the nosetip, which is axisymmetric before the surface ablation commences. The major input parameters are similar to those discussed in Ref. 8 except that angle-of-attack $\alpha$ is approximately 10 deg instead of zero. Before the surface recession, the ratio of the spreading coordinate to the radius from the wind axis is on the order of 1.2 (windward ray) at the surface plug junction. This ratio decreases to a value near unity as the windward region "flattens" with time as a result of higher surface recession along the windward ray. Thus, the effect of streamline spreading is expected to be small and the equivalent-cone approximation[6] may be useful, at least for the nosetips (relatively small values of $s/R_N$). Figures 11 and 12, respectively, show at time $A$ the pressure and heat transfer coefficient contours as projected

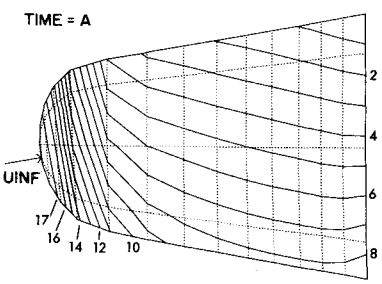


**Fig. 11 Example of pressure contour.**

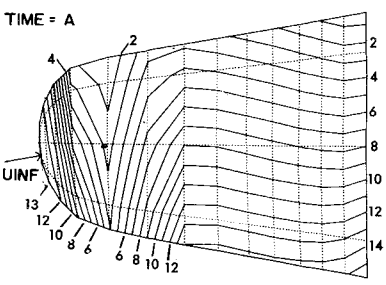


**Fig. 12 Example of heat transfer coefficient contour.**

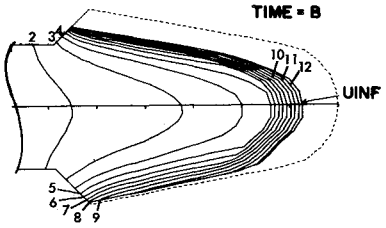


Fig. 13 Example of shape and isotherm, $\phi = 0$–$180°$.

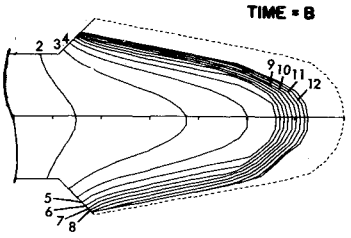


Fig. 14 Example of shape and isotherm, $\phi =$ 45–135°.

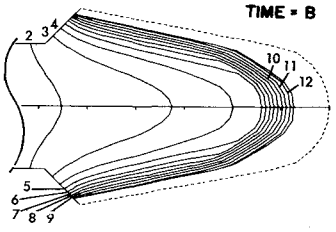


Fig. 15 Example of shape and isotherm, $\phi = 90°$.

onto the pitch plane of symmetry. The curve indices are proportional to the logarithms of the variables. The location of transition may be observed in Fig. 12. Example shapes and isotherms at time $B(B > A)$ are given in Figs. 13–15, respectively, for $\phi = 0$–$180°$, 45–135°, and 90° planes. The isotherm indices are proportional to the temperature. It is seen that in the nose region, for this constant $\alpha$ case, the ablated shape and isotherm are approximately symmetrical with respect to the wind axis. Downstream, however, considerably more side-wall recession occurs along the windward ray. A significant asymmetry is also developed in the internal temperature field.

It is seen from the results presented that relatively coarse grids may be used for GRANT3D computations. This results in a significant reduction in computer run time. For axisymmetric problems, for instance, typical GRANT3D run time is one-fourth of that required by the previous 2-D GRANT code.[4] Results from the GRANT3D code may be coupled to a 3-D stress calculation and provide a practical design analysis for nosetip at angle of attack.

## References

[1] Thyson, N., Neuringer, J., Pallone, A., and Chen, K. K., "Nose Tip Shape Change Predictions During Atmospheric Re-Entry," AIAA Paper 70-827, Los Angeles, Calif., 1970.

[2] Popper, L. A., Toong, T. Y., and Sutton, G. W., "Three-Dimensional Ablation Considering Shape Change and Internal Heat Conduction," *AIAA Journal*, Vol. 8, Nov. 1970, pp. 2071–2074.

[3] Gallagher, L. W., Coleman, W. D., and Butler, W. R., "Advanced Composites II (RESEP II), CO No. P001, Vol. I, Computer User's Manual, Response of Charring Ablator Nosetips—Version 2," LMSC N-16-69-6, SAMSO-TR-70-16, Vol. 1, Sept. 1969, Lockheed Missiles & Space Co., Sunnyvale, Calif.

[4] Chin, Jin H., "Coupling of Shape Change, Heating Distribution and Internal Conduction for Ablating Bodies," *AIAA Progress in Astronautics and Aeronautics: Fundamentals of Spacecraft Thermal Design*, Vol. 29, edited by John W. Lucas, The MIT Press, Cambridge, Mass., 1972, pp. 333–347.

[5] Gallagher, L. W., Coleman, W. D., and Hearne, L. F., "Nosetip Design Analysis and Test Program (NDAT), Vol. III. Computer User's Manual for the Contour Change of Ablating Nosetips (COCAN)," LMSC-D030054, SAMSO-TR-71-11, Dec. 1970, Lockheed Missiles & Space Co., Sunnyvale, Calif.

[6] Baker, R. L., "Low Temperature Ablator Nosetip Shape Change at Angle of Attack," AIAA Paper 72-90, San Diego, Calif., 1972.

[7] Chen, K. K., "Three-Dimensional Nosetip Shape Changes in Hypersonic Flow, Part I: Illustration of a Mathematical Model-Characteristic Method," AIAA Paper 73-762, Palm Springs, Calif., 1973.

[8] Schneider, P. J., Teter, R. D., Coleman, W. D., and Heath, R. M., "Design of Graphite Nosetips for Ballistic Re-Entry," *Journal of Spacecraft*, Vol. 10, Sept. 1973, pp. 592–598.

[9] Lipschutz, M. M., *Theory and Problems of Differential Geometry*, McGraw-Hill, New York, 1969, pp. 3–5.

[10] Arpaci, V. S., *Conduction Heat Transfer*, Addison-Wesley, Palo Alto, 1966, pp. 19–26.

[11] Chin, J. H., "Graphite Nosetip Thermal 3-D (GRANT3D) Response Code; Analysis and Computer User's Manual," LMSC-D366946, Nov. 1974, Lockheed Missiles & Space Company, Inc., Sunnyvale, Calif.

[12] Vaglio-Laurin, R., "Laminar Heat Transfer on Blunt-Nose Bodies in Three-Dimensional Hypersonic Flow," WADC TN 58-147, May 1958, Wright Air Development Center, Wright-Patterson Air Force Base, Ohio.

[13] Leigh, D. C. and Ross, B. B., "Surface Geometry of Three-Dimensional Inviscid Hypersonic Flows," *AIAA Journal*, Vol. 7, Jan. 1969, pp. 123–129.

[14] DeJarnette, F. R., "Calculation of Inviscid Surface Streamlines and Heat Transfer on Shuttle Type Configurations," CR-111921, Aug. 1971, NASA.

[15] Widhopf, G. F., "Heat-Transfer Correlations for Blunt Cones at Angle of Attack," *Journal of Spacecraft*, Vol. 8, Sept. 1971, pp. 1002–1004.

[16] Widhopf, G. F., and Hall, R., "Transitional and Turbulent Heat-Transfer Measurements on a Yawed Blunt Conical Nosetip," *AIAA Journal*, Vol. 10, Oct. 1972, pp. 1318–1325.

[17] Smithson, R. E. and Thoren, C. J., "Temperature Tables, Part 6. One-Layer Spherical Segments, External Heating, One-Space Variable, Linear," NAVORD Rept. 5562, Pt. 6, Sept. 1958, Naval Ordnance Test Station, China Lake, Calif.

[18] Haji-Sheikh, A. and Sparrow, E. M., "The Solution of Heat Conduction Problems by Probability Methods," *Journal of Heat Transfer*, Vol. 89C, May 1967, pp. 121–131.

[19] Widhopf, G. F., "Turbulent Heat Transfer Measurements on a Blunt Cone at Angle of Attack," *AIAA Journal*, Vol. 9, Aug. 1971, pp. 1574–1580.

[20] Baker, D. L., Wool, M. R., Powars, C. A., and Derbidge, T. C., "PANT Series C Wind Tunnel Test Data Report," Aerotherm Project 7043, Jan. 1972, Aerotherm Acurex Corp., Mountain View, Calif.

[21] Anderson, A. D., "Analysis of PANT Series A Rough Wall Calorimeter Data, Part II. Surface Roughness Effects on Boundary Layer Transition," Aerotherm Rept. 73-81, Feb. 1973, Aerotherm Acurex Corp., Mountain View, Calif.